Magnetic Resonance Imaging, Vol. 11, pp. 183–196, 1993
Printed in the USA. All rights reserved.

0730-725X/93 $6.00 + .00

● *Original Contribution*

CORRECTION OF INTENSITY NONUNIFORMITY IN MR IMAGES OF ANY ORIENTATION

DAVID A.G. WICKS, GARETH J. BARKER, AND PAUL S. TOFTS
NMR Research Group, Institute of Neurology, London, U.K.

The specialised radiofrequency (RF) coils used in MRI such as head or surface coils can give rise to marked image intensity nonuniformities. There are two situations in which it is essential to correct this: (1) When a global intensity threshold is used to segment particular tissues; and (2) in proton density images, from which the proton concentration can be measured provided that the system gain is uniform or known over the whole image. We describe experiments to determine the magnitude and sources of nonuniformity in a 0.5-T system, and assess methods devised to correct for them in scans of any orientation, including oblique scans at arbitrary angles to the magnet axis and arbitrary offsets from the magnet iso-centre. A correction based on the response of a system to a uniform phantom was implemented. Tests of the correction with orthogonal views demonstrate that the uniformity of images of any orientation can be improved significantly with a correction matrix from just one orientation and still further with two matrices, one axial and the other either coronal or sagittal. We expect further improvements to be possible if gradient coil eddy current effects can be reduced.

Keywords: **RF uniformity; Image intensity correction; Intensity threshold; Proton density.**

INTRODUCTION

The specialised radiofrequency (RF) coils used in MRI such as head or surface coils can give rise to marked image intensity nonuniformities. This is most apparent in images of uniform phantoms, where the signal intensity varies across the field of view and from slice to slice with bright regions, or "hot spots," close to the coil windings. In patient images, these effects may not be so obvious and may be confused with abnormal tissue. There are two situations in which it is essential to correct this: (1) when a global intensity threshold is used to segment particular tissues; and (2) in proton density images, from which the proton concentration can be measured provided that the system gain is uniform or known over the whole image.

When a suitable sequence is used (e.g. $SE_{2000/60}$ on a 0.5-T system), multiple sclerosis (MS) lesions appear brighter than the surrounding tissues, so a threshold method may be employed to segment them. However, nonuniformities at the edge of the field of view can raise the intensity of the grey matter so that it is similar to that of the lesions. The effect is clearly demonstrated by the intensity profile taken from an oblique scan of a patient with MS in Fig. 1. Without correction for the nonuniformities, the grey matter peaks (A) are of a similar height to the lesion peak (B), so a uniformity correction is required.

The nonuniformity is a property of the instrument rather than of the object being imaged, and in principle can be completely described by making measurements on known uniform objects. Having determined the behaviour of the instrument, corrections can be applied to images of the objects under investigation, usually patients.

There are several possible sources of nonuniformity in clinical images:

1. the transmitted B_1 field (which determines flip angle)
2. the received B_1 field (which determines sensitivity)
3. the receiver filter: an analogue filter in the receiver chain used to limit bandwidth and hence prevent aliasing in the frequency encode direction. (This is

RECEIVED 9/24/91; ACCEPTED 8/27/92.
Address correspondence to Dr. David A.G. Wicks, NMR Research Group, Department of Clinical Neurology, Institute of Neurology, Queen Square, London WC1N 3BG, United Kingdom.

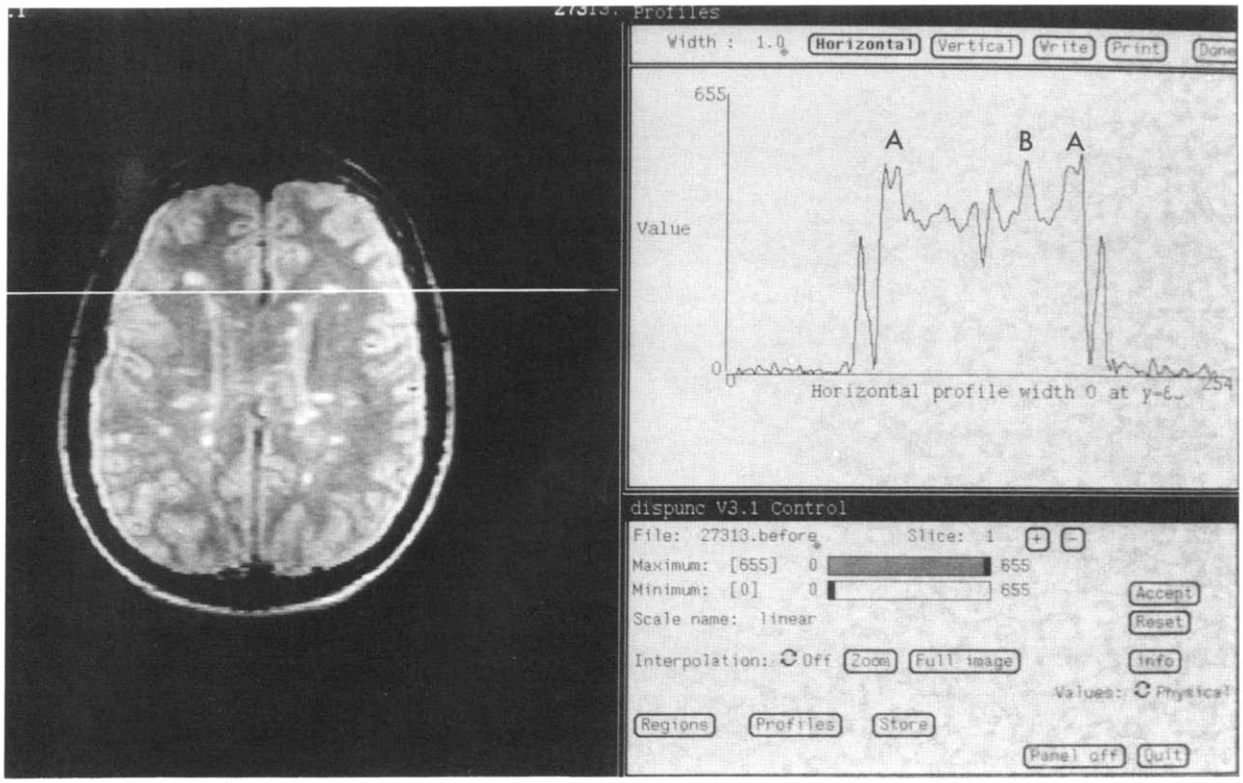

Fig. 1. An intensity profile through a slice from an oblique $SE_{2000/60}$ scan of a patient with multiple sclerosis. Without correction for image intensity nonuniformities the two peaks corresponding to the grey matter (A) are a similar height to the peak from the lesion (B). Thus intensity cannot be used to discriminate normal and abnormal.

distinct from any digital filters which may be used in the image reconstruction process. No digital filters were employed in these experiments.)

4. uncompensated gradient eddy currents, which may cause nonuniformities (e.g., (a) unwanted gradients present during selective pulses will select a slice in a different position from that required, and (b) unwanted time-varying gradients present during the spin echo sequence cause dephasing, which is not refocussed by the 180° pulse and results in signal loss).

McVeigh et al.[1] developed a model of the nonuniformity produced by their head coil by modelling its spatial variation in sensitivity. They demonstrated a similarity between their prediction and the measured nonuniformity with a uniform phantom in a single slice. They then corrected a slice from a patient scan with the phantom data, removing much of the visible nonuniformity. Axel et al.[2] compared a correction based on the response to a uniform phantom to a filtering technique which approximated this response by a highly blurred version of the image to be corrected. The latter removed the need for care in reproducibly positioning the coil and did not require additional scanning of phantoms for different coil positions, but the best corrected images were produced by the phantom method. Furthermore, the filtering technique introduced distortions in the intensity profiles of edges in the corrected image.

A homomorphic filtering method was used by Fuderer and van Est.[3] In an attempt to avoid edge artifacts they removed the image background prior to filtering, but they made no comment on effectiveness of this, nor did they compare it with any other technique. Lim and Pfefferbaum[4] avoided the edge artifacts by extending the intensities of each point on the edge of the object (brain) to the edge of the image matrix. The resultant "feathered" image was devoid of sharp intensity transitions and could then be processed with a low pass filter. This method allowed segmentation of different tissues based only on their intensities.

The most thorough study of the causes of image nonuniformity, its magnitude and possible corrections was carried out by Condon et al.[5] They discovered two major sources of nonuniformity in their system,

the receiver filter applied in the frequency-encode direction and the receiver coil. Two corrections were tried, both based on the signal produced by a uniform phantom. The first processed the phantom with a primitive low pass filter to reduce random noise and used the result as a correction matrix. The second fitted a curve to the horizontal intensity profile of the phantom and another curve to the vertical profile. These curves were then used to correct each point in an image using its known vertical and horizontal displacements from the image centre. Corrections were produced for transverse, coronal, and sagittal views independently. A comparison was made between the two techniques within single slices in each view. The curve fitting technique reduced the measured nonuniformities more effectively than the filtered phantom image which in some cases increased the nonuniformity due to incomplete removal of random noise. Slice-to-slice variations were not studied.

This paper describes experiments to determine the magnitude and sources of nonuniformity in our system, and assesses methods devised to correct for them, in multislice head images of any orientation including oblique.

METHODS

Definition of Nonuniformity

We define image nonuniformity in two ways, one for in-slice nonuniformity and the other for slice-to-slice variations:

In-slice nonuniformity. We define this for a uniform object as the ratio of the standard deviation of the image intensities (σ) to their mean (μ), after sufficient low pass filtering (i.e., smoothing) has been applied to remove random noise:

$$\text{Percentage in-slice nonuniformity} = \frac{\sigma}{\mu} \times 100 \quad . \quad (1)$$

Phantom image intensities were measured from a 160 × 160 mm square region of interest at the center of the 320 mm field of view in each slice. This corresponds to the volume occupied by the brain in typical patient images.

Slice-to-slice nonuniformity. We define this as the ratio of the standard deviation of the individual slice means to their overall mean and calculate it over 32 5-mm slices:

$$\text{Percentage slice-to-slice nonuniformity} = \frac{\sigma_{\text{SliceMean}}}{\mu_{\text{OverallSlices}}} \times 100 \quad . \quad (2)$$

Imaging Sequences and Phantom

All measurements were made on a Picker 0.5 T whole body imager (Picker International, Cleveland, OH). A body coil (56 cm long with 60 × 46 cm elliptical cross section) and a head coil (25 cm long with 29 cm circular cross section) were available. Both coils were of saddle design. The body coil was always used for transmission, to produce a relatively uniform RF field, but either of the coils could be used for reception. Their longitudinal positions were measured with respect to the magnet center. The body coil was always centered and the head coil was usually positioned less than 20 mm from the center.

A doped water phantom which just filled the volume of the head coil was imaged using a multislice $SE_{2000/60}$ sequence with a 320 mm field of view, two excitations and 32 contiguous 5-mm slices collected in an interleaved fashion (i.e., first all the odd slices then all the even ones). As no standard phantom provided by the manufacturer was large enough to fill the coil completely, a phantom was constructed from a polythene sack filled with doped water and supported in a bucket. The phantom was not completely rigid and gave a noncircular cross section in transverse images. Folds in the inner sack are also visible at the ends of the phantom in some images but as these lie outside the volume normally occupied by the head they are not important. The transverse image in Fig. 2 clearly shows the intensity nonuniformities produced by the system with four hot spots near the head coil windings.

Post Processing

All post processing of images including the uniformity correction was carried out off-line on Sun workstations (Sun Microsystems, Inc., Mountain View, CA). All the techniques were implemented in the C language and were based around the UNC image processing library (University of North Carolina, Chapel Hill, NC). Images were displayed with the Dispimage program (David Plummer, University College Hospital, London) and results plotted using Grtool (Paul Turner, Oregon Graduate Institute).

Determination of the Sources of Significant Nonuniformities

The effect of the receiver filter. The effect of the filter can be isolated and measured by collecting images with no object present (i.e., by scanning air) so that the effects of RF and magnetic nonuniformities are removed. Random white noise is collected, which is uniformly distributed in frequency space, and hence is uniform in the image apart from the effect of any filtering. In a magnitude reconstruction, the mean value

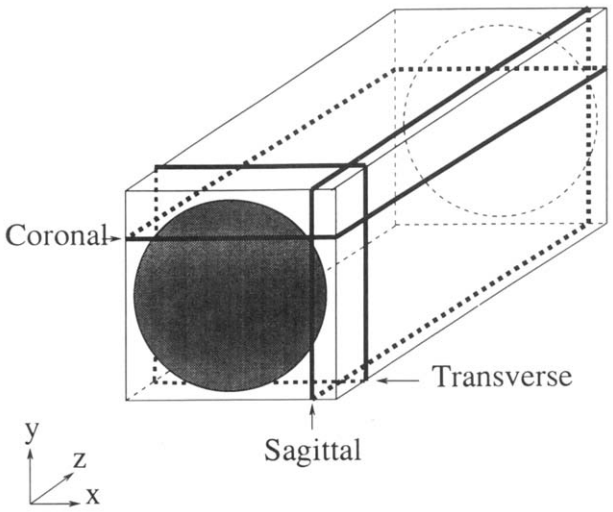

(A)

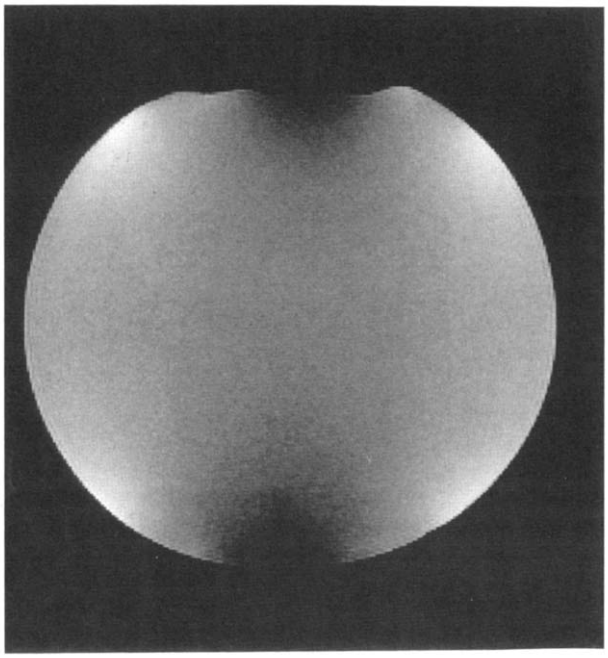

(B)

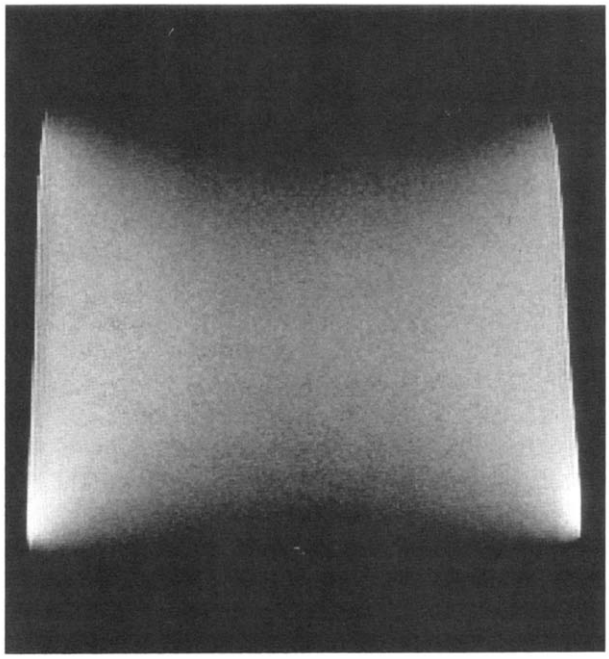

(C)

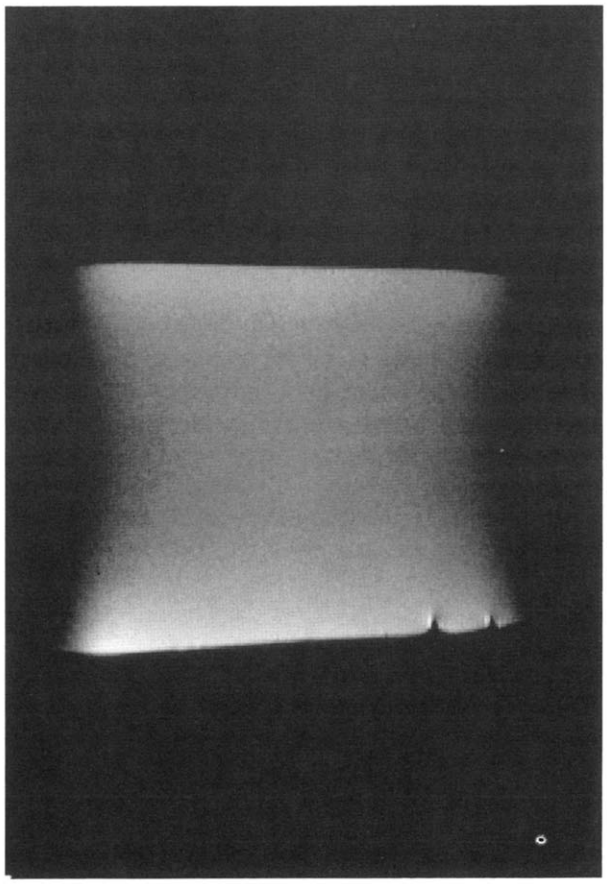

(D)

Fig. 2. Views of the uniform phantom from an $SE_{2000/60}$ using the body coil to transmit and the head coil to receive. The slices were selected to show the nonuniformity "hot spots": (A) schematic of slice positions, (B) transverse slice, (C) coronal slice, and (D) sagittal slice.

in a pixel is proportional to the noise,[6] and hence may be used as a measure of the relative filter response at that position in the image.

Images were collected with a series of filters of bandwidth 1–30 kHz. The signal bandwidth in the frequency encode direction (determined by the sampling rate) was set to be much larger than that of the filter in each case, so that the filter's effect could be easily observed and the unknown filter function determined. A spatial domain function of the form proposed by Condon et al.[5] was found to be a close estimate to the effects observed:

$$I = I_0 \exp\left\{ -k\left[\frac{\omega_{FE} d}{\omega_F fov} \right]^2 \right\} \quad (3)$$

where

I = image intensity
I_0 = image intensity at image slice center
k = empirically derived constant for all filter bandwidths
ω_{FE} = bandwidth of frequency-encode direction (determined by the sampling rate)
ω_F = filter bandwidth (stated by manufacturer)
d = displacement from image center in frequency-encode direction
fov = field of view size (in same units as d, e.g., pixels).

A typical frequency-encode bandwidth of 12 kHz and a 10.5 kHz filter produce a 21% drop in intensity from the center to the edge of the image. Figure 3 shows noise profiles and their fits along the frequency-encode direction from images collected with filters of bandwidths from 5 kHz to 30 kHz.

The effect of the transmitted and received B_1 fields. The uniform phantom was imaged in the transverse orientation with two different RF coil configurations: (1) the body coil for both transmission and reception (with head coil removed) and (2) the body coil for transmission and head coil for reception. In configuration (1) we expect the nonuniformity arising from the coil to be relatively small, since even the extremities of the phantom are not far from the coil's center. The difference between configurations (1) and (2) gives an indication of the extra nonuniformity arising from using the head coil as a receiver.

The measured nonuniformities are shown in Table 1 and Fig. 4. In all cases there was an overall decrease in signal moving away from the center slice. The in-slice nonuniformity was low with a mean of 3% when using the body coil for reception (configuration 1), as expected. This indicates that in the slice plane (in the transverse orientation) there are no significant eddy current problems and the transmitted RF field is uniform. Using the head coil for reception (configuration 2), in-slice nonuniformity increased to a mean of 10% and hot spots were visible close to the coil windings, again as expected. This indicates that in configuration 2, the major source of in-slice nonuniformity is the variation in the received B_1 field of the head coil. Slice-to-slice nonuniformity with the body coil was only 3.8%, but was degraded to 7.8% with the head coil, because of its shorter axial dimension. With both coils there was significant odd–even slice-to-slice nonuniformity (see Fig. 4). This effect has been described in detail by Johnson et al.[7] who attributed it to gradient eddy currents.

Corrections for Nonuniformities in Scans of Any Orientation

Oblique multislice scans are used routinely when imaging the brain, so it was important to devise corrections that would be applicable to any image orientation. As three major sources of nonuniformity had been detected (i.e., the receiver filter, eddy currents and the RF coils), three types of correction were employed.

Receiver filter correction. This correction employed the inverse of Eq. (3) solved for I/I_0 to correct for all possible combinations of frequency encode and filter bandwidths available on the imager.

Table 1. Nonuniformity in the transverse view with two body and head coil configurations

	Nonuniformity (%)	
Configuration	In-slice mean (range)	Slice-to-slice
(1) Body coil transmit/receive, Head coil removed	2.8 (2–3.6)	3.8
(2) Body coil transmit, Head coil receive	10.1 (8.4–13.4)	7.8

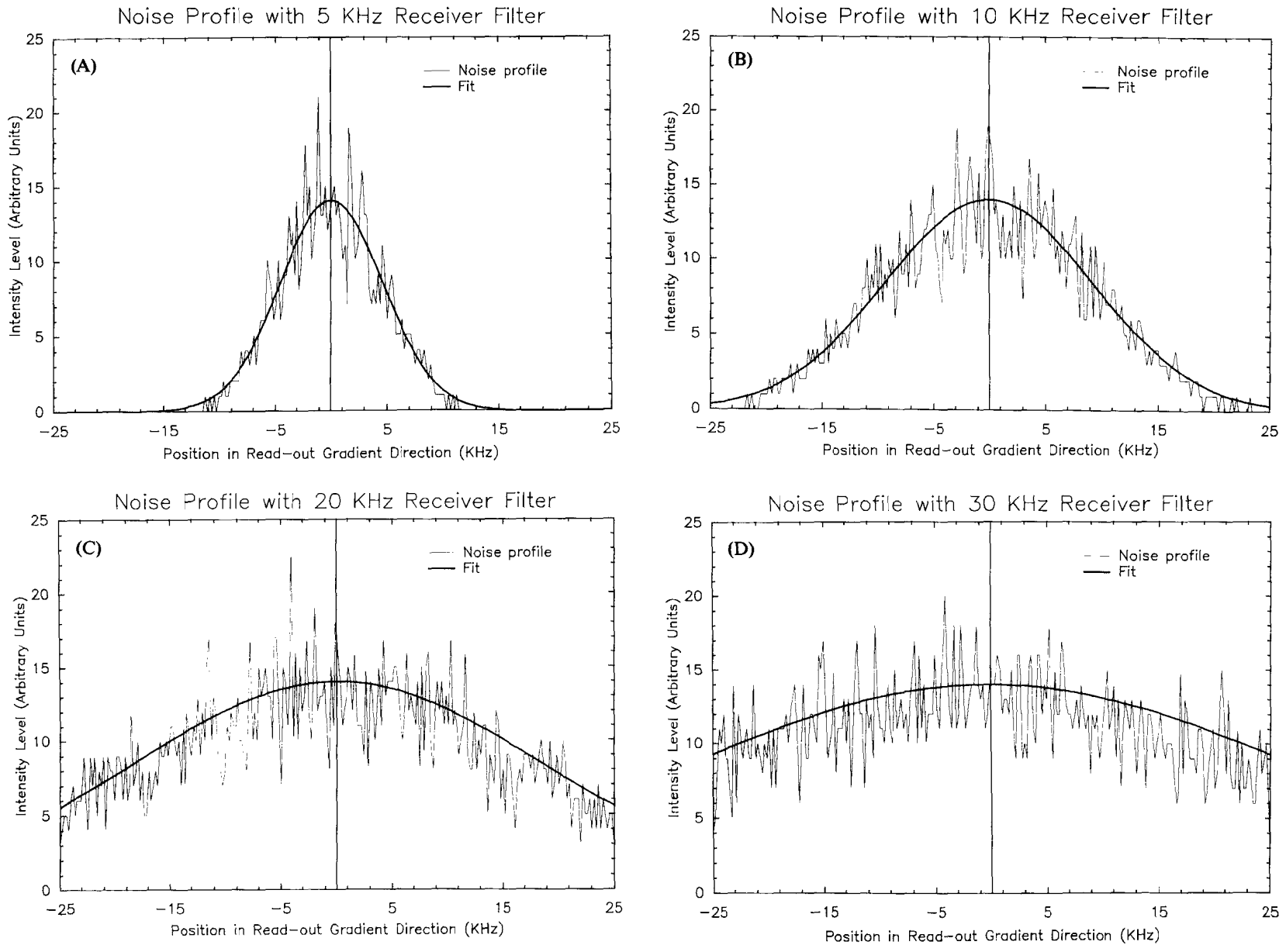

Fig. 3. Noise profiles and their fits along the frequency-encode direction from images collected with receiver filters of bandwidths: (A) 5 kHz, (B) 10 kHz, (C) 20 kHz, and (D) 30 kHz.

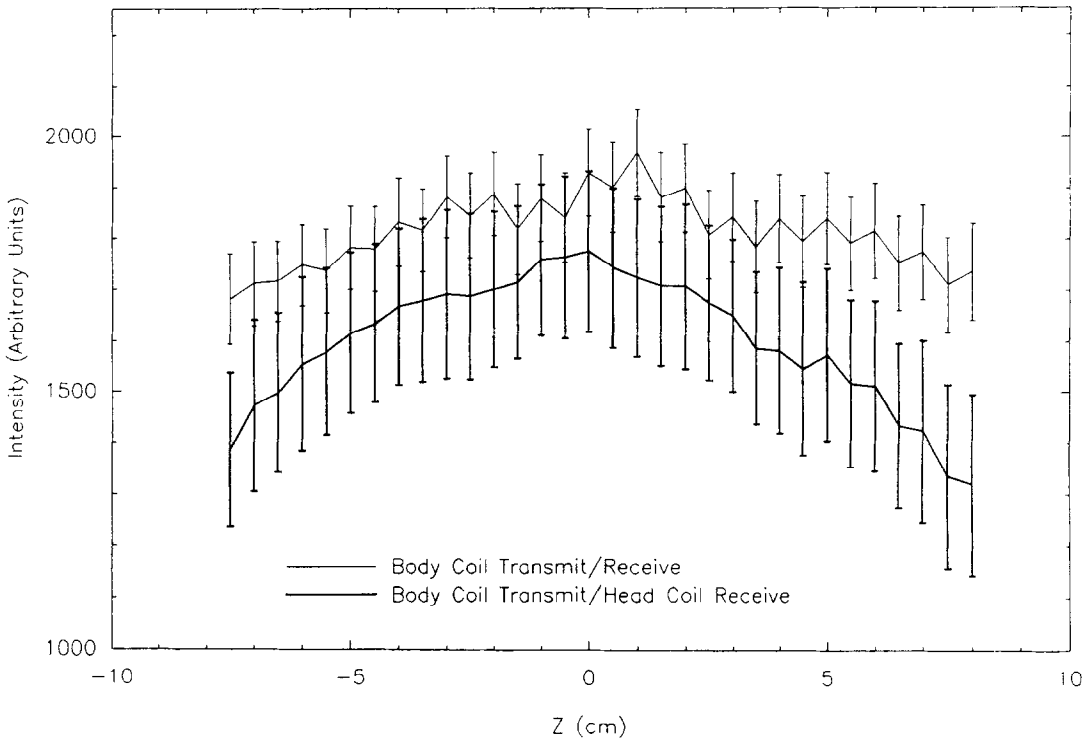

Fig. 4. The nonuniformity along the magnet bore (Z direction) as determined from the transverse view with two different body and head coil configurations (body coil length = 56 cm, head coil length = 25 cm). The mean slice intensities are shown together with error bars corresponding to ±1 standard deviation. The slice separation is 5 mm.

Eddy current correction. The most distinct effect of eddy currents was the odd–even slice intensity variations. This was corrected in the phantom images by rescaling the intensities in each slice with a running average of the intensity of seven consecutive slices calculated over a small circular region of interest. The region was positioned well away from the hot spots produced by the receiver coil to minimise its influence on the correction. The correction removed the sharp changes of intensity from slice-to-slice without changing the overall shape of the response. The remaining nonuniformity is mainly due to the RF coils, although there is still probably a small component from eddy current effects. It should be noted that this correction does not address any in-slice intensity variations produced by eddy current effects.

RF coil correction. As noted previously, three possible approaches have been used for correction of the RF coil nonuniformities[1–5]:

1. correction matrix produced from a uniformity phantom;
2. correction matrix produced from a mathematical model of coil spatial response;
3. high pass filtering.

Approach (2) does not correct for effects arising from coil imperfections; approach (3) removes any genuine low and zero spatial frequency signal that may be present in addition to the nonuniformities. We therefore chose to implement approach (1), which determines the actual nonuniformities shown in an image of a uniform phantom and use this image to produce a correction matrix which can be divided from a patient or object image to correct for its nonuniformities.

Formation of the correction matrix. The formation of a correction matrix from a raw phantom image was carried out in several stages. First the effects of the receiver filter and eddy currents were removed from the image as described in the previous sections on receiver filter correction and eddy current correction. Then, to correct for oblique imaging planes, the physical coordinates of the phantom image were transformed to match those of the patient/object image:

$$P'(x, y, z) = [T] \cdot P(x, y, z) \tag{4}$$

where P' = phantom image viewed from the same position as the oblique patient/object image, P = phantom image in its original position, and

$$[T] = [\text{ObjectShifts}]\,[\text{ObjectRotations}] \times [\text{PhantomRotations}]^{-1}\,[\text{PhantomShifts}]^{-1}. \quad (5)$$

T is a 4 × 3 transformation matrix derived from the 3-dimensional offsets and rotations of the phantom and patient/object images with respect to the magnet coordinate system. This information is recorded in the header of the image files by the manufacturer's software. The transformed phantom image was mapped back onto the discrete 3-dimensional image grid by trilinear interpolation.

The accuracy of the figures recorded by the manufacturer's software and of the transformation software was checked with a resolution phantom scanned at a number of different orientations and offsets. The largest error was 2 pixels, equivalent to a shift of 2.4 mm, which is acceptable since intensity changes due to nonuniformity are negligible over this distance.

Two problems have been reported with phantom based corrections, namely the need for different scans for different coil positions and the introduction of random noise from the phantom image. Since both phantom and patient/object scans are centered in the body coil where nonuniformities arising from the transmitted field are low, it should only be necessary to correct for nonuniformities arising from the received field of the head coil. This coil can move in only one direction (along the bore of the magnet) and its displacement from the magnet/body coil center, which can easily be measured, is usually less than 20 mm. As the position of any scan with respect to the magnet center is recorded by the manufacturer's software, the relative position of the scan and the head coil and the scan center is also known. Thus, only one scan is required to measure the nonuniformity pattern produced by the body coil/head coil configuration and this may be shifted with respect to the patient scan to take into account different head coil positions.

Random noise was removed from the phantom image with a 2-dimensional median filter applied to each slice. This filter has been compared with a wide range of spatial filters by Chin and Yeh[8] and Mastin,[9] who showed that it reduced random noise and preserved real image features the most effectively. The optimum filter size was derived experimentally from the in-slice nonuniformity of a phantom image which had been processed with a range of median filters from 3 × 3 to 11 × 11. As the size of the filter increased from 3 × 3 to 7 × 7, the apparent in-slice non-uniformity (σ/μ) was reduced due to the removal of random noise. There was no further reduction with the 9 × 9 or 11 × 11 filters however, so we can conclude that with a filter size of 7 × 7 or greater, random noise made no measurable contribution to the in-slice nonuniformity. The instrumental nonuniformities were unaffected by the filters due to the latters' relatively small size. The span of the 7 × 7 filter was 8 mm with an image resolution of 1.125 mm/pixel.

It should be noted that, although eddy current effects are corrected in the phantom image, the resultant correction matrix does not correct nonuniformity due to eddy currents in the patient/object image, which may vary with slice orientation.

Correction Tests

The uniform phantom was positioned in the center of the head coil, body coil and magnet, and scanned in the transverse, coronal and sagittal orientations (TRAN1, COR1, SAG1). All scans were filtered with a 7 × 7 median filter to remove the random noise and corrected for the effects of the receiver filter. To investigate the possibility of using a single correction matrix to correct for all possible orientations, a matrix was derived from TRAN1 and employed to correct COR1 and SAG1. A matrix was also derived from SAG1 and used to correct COR1. An orthogonal image is the most difficult case of oblique image to correct.

In addition, similar scans in the same orientations were obtained several months later (TRAN2, COR2, SAG2). Correction matrices derived from the old scans were then used to correct the new scans of the same orientation (e.g., matrix from TRAN1 was used to correct TRAN2).

RESULTS

Graphs of slice means and standard deviations before and after correction are shown for each view in Figs. 5 and 6. Each orientation has its own characteristics due to its relative orientation to the RF coils. The transverse view produces a peak intensity at the center slice with relatively little variation in standard deviations. The coronal view produces little variation in slice means but standard deviations increase substantially with distance from the center. The sagittal view is characterised by a minimum intensity at the center slice with little variation in the standard deviations.

Correction With Matrices From Orthogonal Views

Correction of COR1 with the matrix derived from TRAN1 reduced the maximum in-slice nonuniformity from 18.9% to 8.7% and the minimum from 8% to 6% (Table 2). There was little change in the slice-to-slice nonuniformity. Correction of COR1 with the matrix derived from SAG1 was more successful, however, reducing the maximum in-slice nonuniformity to 4.7%

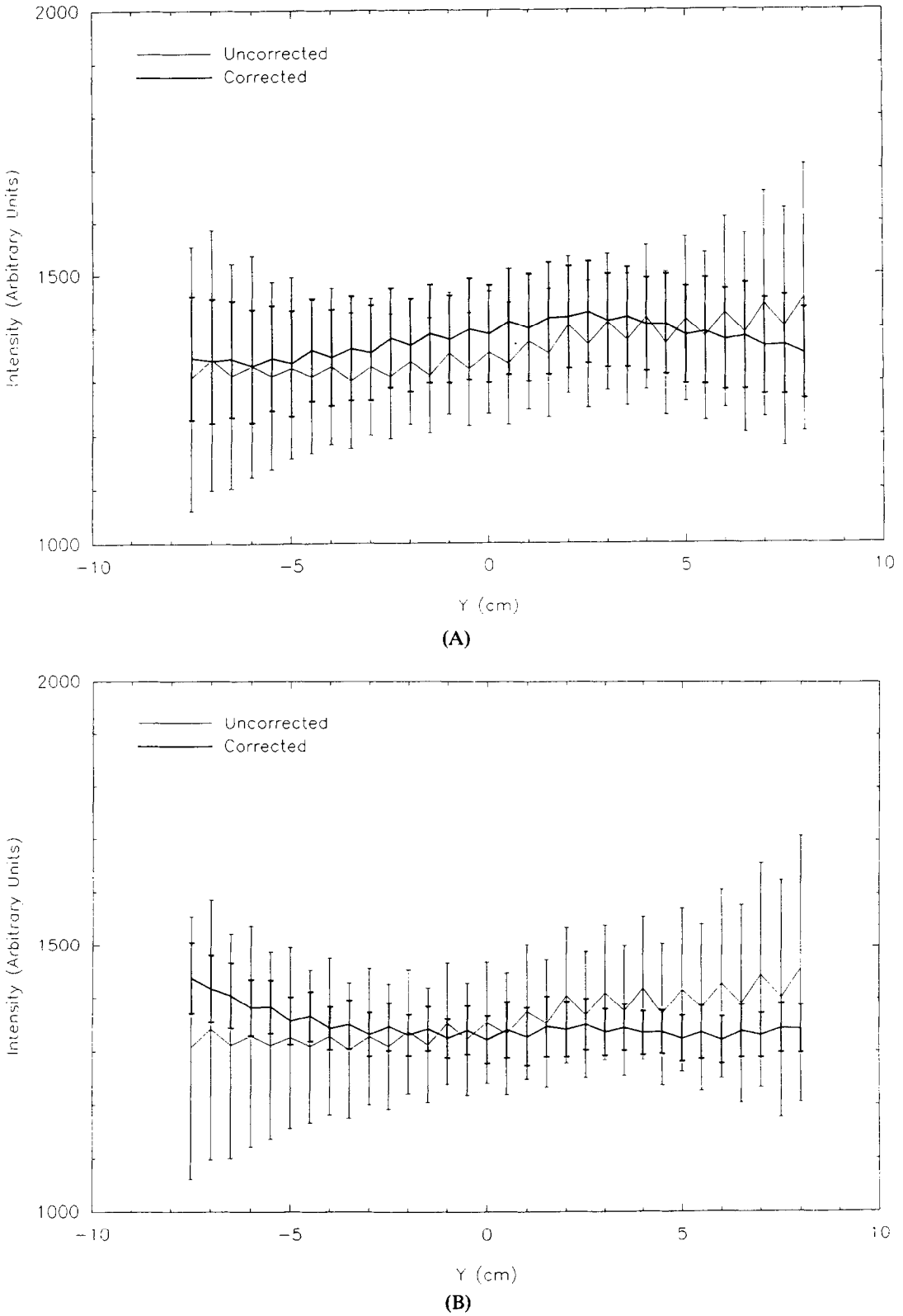

Fig. 5. Nonuniformities with head receiver coil before and after correction with an orthogonal view. The intensity values are the mean intensity from a 160 × 160 mm region of interest in each slice. The error bars are the corresponding standard deviation. *X*, *Y* and *Z* are the horizontal (perpendicular to bore), vertical and horizontal (along bore) directions with respect to the magnet. (A) COR1 corrected by the matrix from TRAN1 and (B) COR1 corrected by the matrix from SAG1. (*Figure continues*)

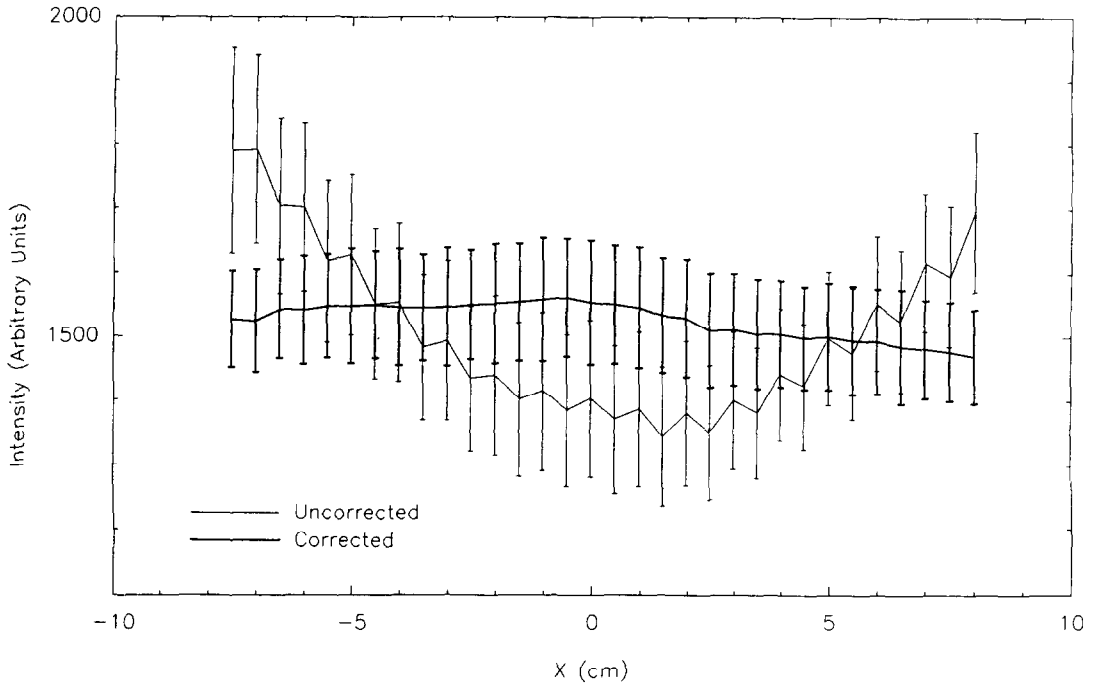

(C)

Fig. 5 continued. (C) SAG1 corrected by the matrix from TRAN1.

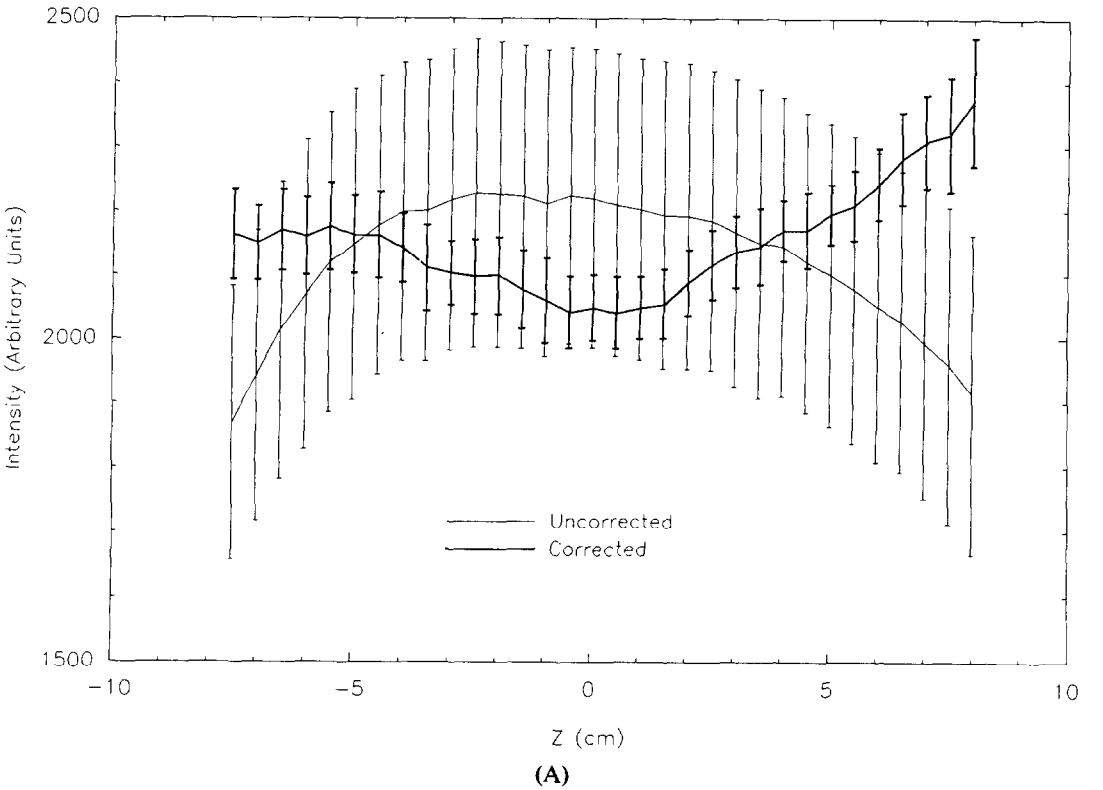

(A)

Fig. 6. Nonuniformities with head receiver coil before and after correction with the same view. The intensity values are the mean intensity from a 160 × 160 mm region of interest in each slice. The error bars are the corresponding standard deviation. *X*, *Y* and *Z* are the horizontal (perpendicular to bore), vertical and horizontal (along bore) directions with respect to the magnet. (A) TRAN2 corrected by the matrix from TRAN1. (*Figure continues*)

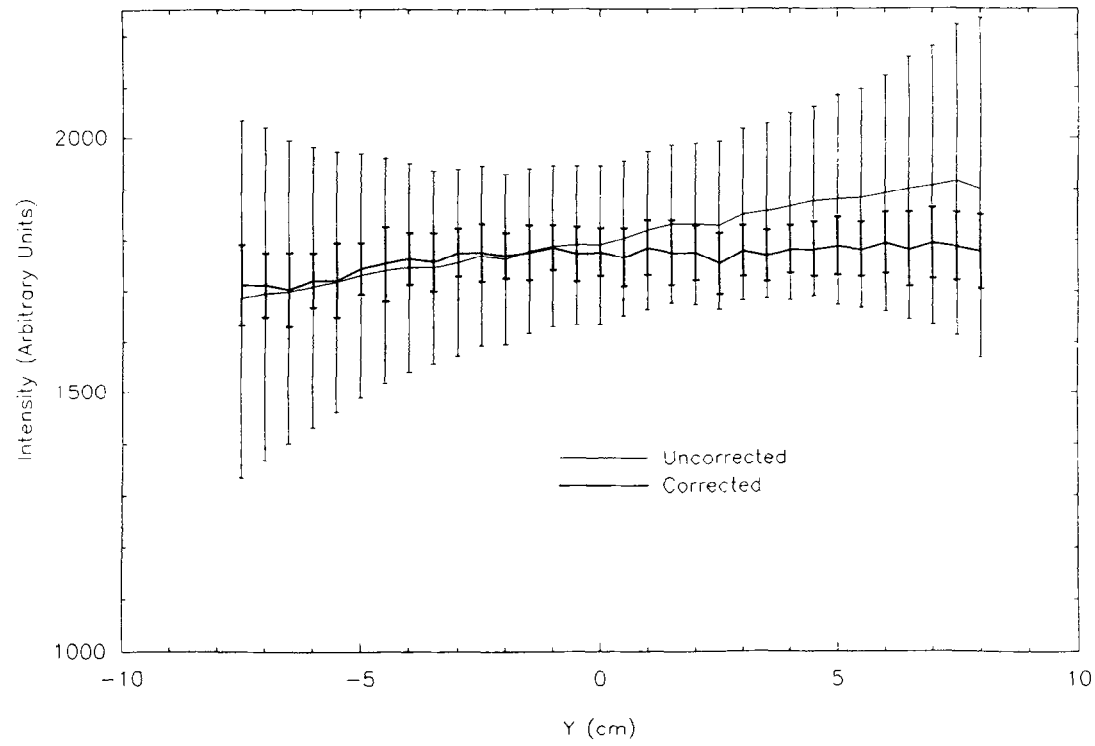

(B)

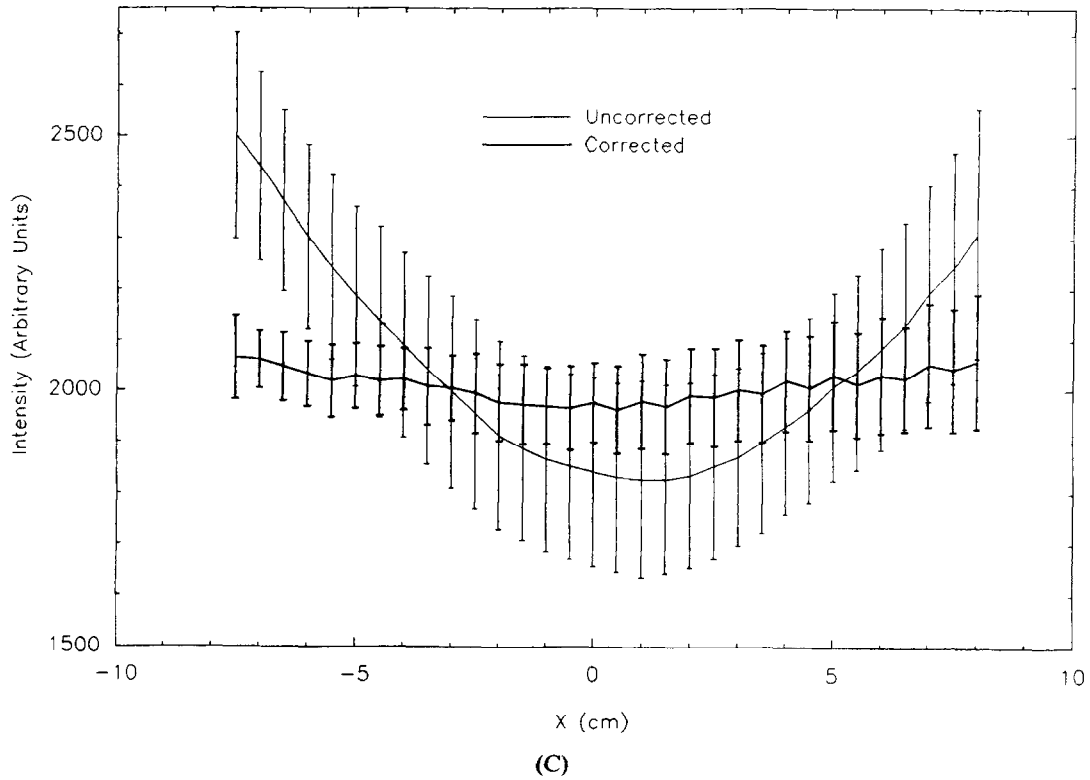

(C)

Fig. 6 continued. (B) COR2 corrected the matrix from COR1, and (C) SAG2 corrected by the matrix from SAG1.

Table 2. Correction with matrices from orthogonal views

View	View used to derive correction	Nonuniformity measure (%)			
		In-slice		Slice-to-slice	
		Before correction mean (range)	After correction mean (range)	Before correction	After correction
COR1	TRAN1	11.4 (8–18.9)	7 (6–8.7)	3.2	2.0
COR1	SAG1	11.4 (8–18.9)	3.5 (2.8–4.7)	3.2	2.0
SAG1	TRAN1	7.8 (6.6–9)	5.7 (4.9–6.2)	8.5	1.8

and the minimum to 2.8%. Correction of SAG1 with the matrix from TRAN1 reduced the slice-to-slice nonuniformity from 8.5% to 1.8% but had little effect on the smaller in-slice nonuniformities.

Correction With Matrices From the Same View

The mean in-slice nonuniformity of TRAN2 was reduced from 11.2% to 2.8% by the matrix from TRAN1, but the slice-to-slice nonuniformity only changed from 4.8% to 3.9% (Table 3). This was probably due to a slight uncorrected offset in the head coil position along the magnet axis for the second scan. When COR2 was corrected by the matrix from COR1 the in-slice nonuniformity was reduced from 12.5% to 3.3% and slice-to-slice from 3.9% to 1.4%. The in-slice nonuniformity in SAG2 corrected by the matrix from SAG1 was reduced from 10.4% to 4.3% and slice-to-slice nonuniformity was reduced from 9.4% to 1.5%.

Correction of an Oblique Patient Scan

The image in Fig. 1 showing the effects of nonuniformity in an oblique scan of a patient with MS, was corrected using the matrix derived from TRAN1. The intensity profile after correction, in Fig. 7, shows grey matter peaks (A) corrected to lower values and one clear peak (B) corresponding to the lesion. Thus this technique removes nonuniformities sufficiently to allow lesion segmentation with a threshold even in oblique scans.

DISCUSSION

Correction of coronal and sagittal views using a correction matrix derived from the transverse view produced dramatic reductions in the nonuniformities, especially when these were initially particularly large. Correction with matrices derived from the same orientation was even more effective, however, as was the correction of the coronal view by the matrix derived from sagittal view. The latter was probably due to the fact that both views are orientated radially with respect to the magnet bore and the effect of eddy currents is similar.

Therefore, correction of orientation dependent nonuniformities could be improved by the use of two correction matrices, one transverse and the other coronal or sagittal. Scans would be corrected by the matrix most closely aligned. The effectiveness of this approach has been demonstrated by the correction of the near transverse oblique scan with the matrix derived from TRAN1 shown in Figs. 1 and 7 where the correc-

Table 3. Correction with matrices from the same view scanned at different times

View	View used to derive correction	Nonuniformity measure (%)			
		In-slice		Slice-to-slice	
		Before correction mean (range)	After correction mean (range)	Before correction	After correction
TRAN2	TRAN1	11.2 (10.4–13)	2.8 (2.1–4.2)	4.8	3.9
COR2	COR1	12.5 (9.2–21.3)	3.3 (2.5–4.6)	3.9	1.4
SAG2	SAG1	10.4 (9–12.3)	4.3 (2.8–6.4)	9.4	1.5

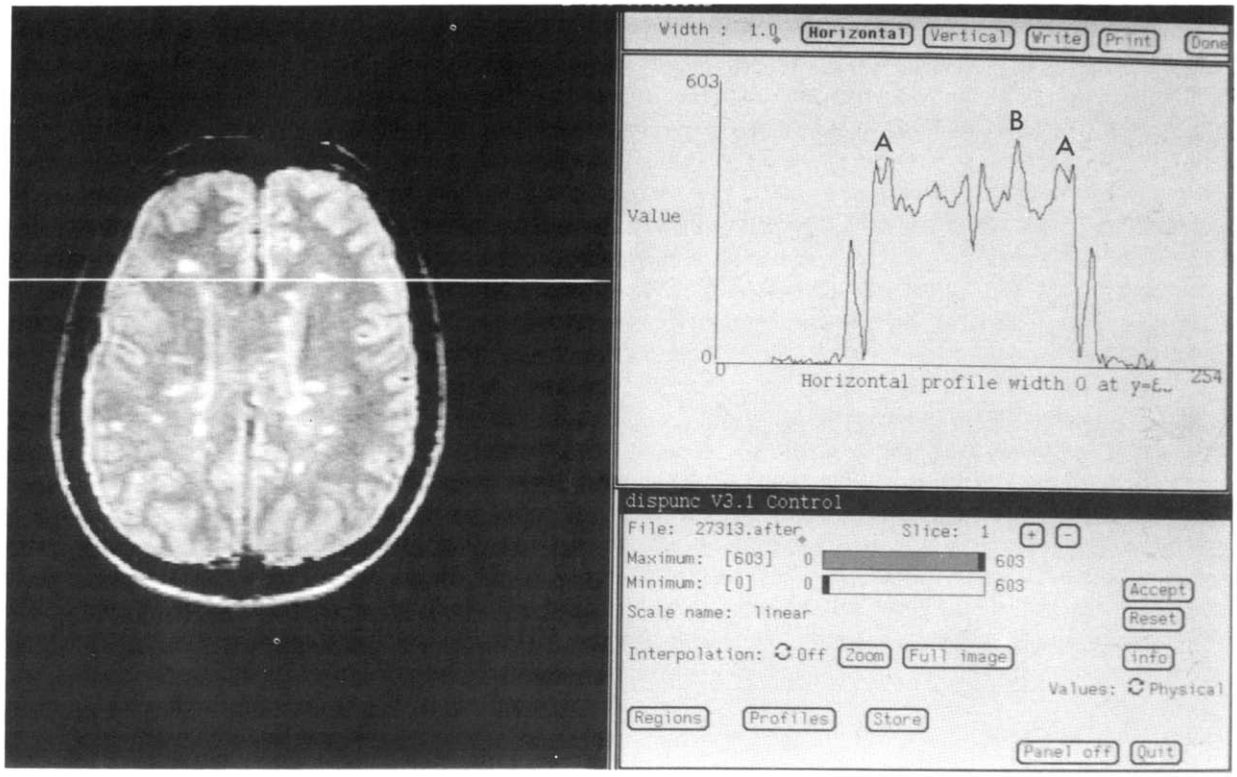

Fig. 7. An intensity profile through a slice from an oblique $SE_{2000/60}$ scan of a patient with multiple sclerosis. After correction for image intensity nonuniformities the two peaks corresponding to the grey matter (A) are lower in height than the peak from the lesion (B). Thus intensity can now be used to discriminate normal and abnormal.

tion was sufficient to remove the ambiguity between the intensity peaks due to lesion and grey matter.

A more ideal correction for oblique scans would be to acquire a phantom image in exactly the same orientation. The failure of the correction matrix from the same view to completely correct nonuniformity in these experiments (see Table 3) suggests that, in our case, scanner instability is significant.[10] However, even on more stable systems where the technique would be more effective, it introduces a time penalty which would be unacceptable at most sites. The number of correction matrices employed in any given case will depend on the required image uniformity but the use of two scans should be sufficient in most cases.

We have attempted to correct for the movement of the head coil along the magnet bore by shifting the correction matrix by the same amount. This procedure assumes any correction required for the body coil is small, and does not vary significantly over the distance moved by the head coil. Ideally, all patient scans should be taken with the head coil in the same position, so that better correction for the body coil can be obtained.

Correction for tip angle nonuniformity is made in this scheme, provided that it does not vary with time. This will be the case if the phantom has similar loading characteristics to the patients, and the RF power is always adjusted to take account of any changes in this loading.

This correction technique removes a substantial amount of image nonuniformity, most probably arising from the RF coils, but does not remove the orientation dependent nonuniformities due to eddy currents. Thus, in order to improve image intensity uniformity further, eddy currents should be reduced as much as possible by using good pre-emphasis and shielded gradients, if available.

CONCLUSIONS

The uniformity of images of any orientation can be improved significantly with a correction matrix from just one orientation and still further with two matrices, one axial and the other either coronal or sagittal. We expect further improvements to be possible with the reduction of gradient eddy currents.

Acknowledgments—We wish to thank Dr. R. Robb and the Biodynamics Research Group at the Mayo Clinic, Rochester for AN-

ALYZE which enabled us to carry out a preliminary study into intensity nonuniformities, Professor W.I. McDonald for his support and encouragement and the Multiple Sclerosis Society of Great Britain and Northern Ireland for their considerable financial support.

REFERENCES

1. McVeigh, E.R.; Henkelman, R.M.; Bronskill, M.J. Non-uniform sensitivity of receiver coils in MR imaging. *Abstracts of the SMRM* 4:206; 1985.
2. Axel, L.; Costantini, J.; Listerud, J. Intensity correction in surface-coil imaging. *Am. J. Roentgenol.* 148:418–420; 1987.
3. Fuderer, A.; van Est, A. Surface coil correction using homomorphic filtering. *Abstracts of the SMRM* 6:266; 1987.
4. Lim, K.O.; Pfefferbaum, A. Segmentation of MR brain images into cerebrospinal fluid spaces, white, and grey matter. *J. Comput. Assist. Tomogr.* 13:588–593; 1989.
5. Condon, B.R.; Patterson, J.; Wyper, D.; Jenkins, A.; Hadley, D.M. Image non-uniformity in magnetic resonance imaging: Its magnitude and methods for correction. *Br. J. Radiol.* 60:83–87; 1987.
6. Tofts, P.S., Johnson, G. Correction for Rayleigh noise in an NMR magnitude image when measuring T_2 at low values of signal to noise ratio. *Abstracts of the SMRM* 5:1450; 1986.
7. Johnson, G.; Ormerod, I.E.C.; Barnes, D.; Tofts, P.S.; MacManus, D. Accuracy and precision in the measurement of relaxation times from nuclear magnetic resonance images. *Br. J. Radiol.* 60:143–153; 1987.
8. Chin, R.T.; Yeh, C.L. Quantitative evaluation of some edge preserving noise smoothing techniques. *Computer Vision, Graphics and Image Processing* 23:67–91; 1983.
9. Mastin, G.A. Adaptive filters for digital image noise smoothing: An evaluation. *Computer Vision, Graphics and Image Processing* 31:103–121; 1985.
10. Barker, G.J.; Tofts, P.S. Semi-automated quality assurance for quantitative magnetic resonance imaging. *Magn. Reson. Imaging* 10(4):585–595; 1992.